View Online

This article is published as part of the *Dalton Transactions* themed issue entitled:

Synthetic Solid State Chemistry

Guest Editor Duncan Gregory
University of Glasgow, UK

Published in issue 26, 2010 of *Dalton Transactions*

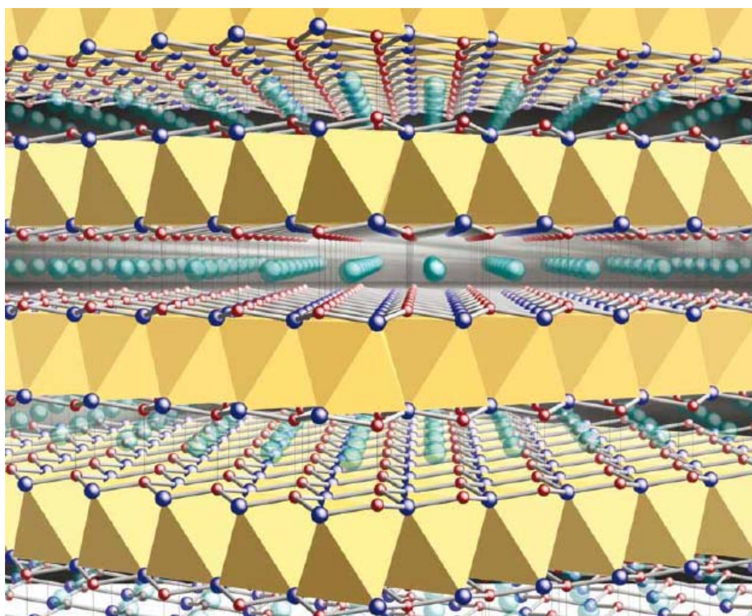

Image reproduced with the permission of Svilen Bobev

Downloaded by Massachusetts Institute of Technology on 22 October 2011
Published on 01 June 2010 on http://pubs.rsc.org | doi:10.1039/C002928A

Articles in the issue include:

PERSPECTIVES:

Syntheses and characterization of some solid-state actinide (Th, U, Np) compounds
Daniel E. Bugaris and James A. Ibers,
Dalton Trans., 2010, DOI: 10.1039/b927026d

Hybrid materials through linkage of chalcogenide tetrahedral clusters
Paz Vaqueiro, *Dalton Trans.,* 2010, DOI: 10.1039/c000130a

COMMUNICATIONS:

Increasing the dimensionality of hybrid vanadium oxyfluorides using ionothermal synthesis
Farida Himeur, Phoebe K. Allan, Simon J. Teat, Richard J. Goff, Russell E. Morris and Philip Lightfoot, *Dalton Trans.,* 2010, DOI: 10.1039/c000318b

One-step synthesis of high-purity fluorous-capped inorganic nanoparticles
Rakesh Voggu, Ajmala Shireen and C. N. R. Rao,
Dalton Trans., 2010, DOI: 10.1039/b927355g

Visit the *Dalton Transactions* website for more cutting-edge inorganic and solid-state research
www.rsc.org/dalton

Factors controlling material deposition in the CVD of nickel sulfides, selenides or phosphides from dichalcogenoimidodiphosphinato complexes: deposition, spectroscopic and computational studies†

Arunkumar Panneerselvam,[a] Ganga Periyasamy,[b] Karthik Ramasamy,[a] Mohammad Afzaal,[a] Mohammad A. Malik,[a] Paul O'Brien,*[a] Neil A. Burton,[b] John Waters[a] and Bart E. van Dongen[c]

Received 11th February 2010, Accepted 12th May 2010
First published as an Advance Article on the web 1st June 2010
DOI: 10.1039/c002928a

Downloaded by Massachusetts Institute of Technology on 22 October 2011
Published on 01 June 2010 on http://pubs.rsc.org | doi:10.1039/C002928A

The series of nickel dichalcogenoimidodiphosphinates $[Ni\{^iPr_2P(X1)NP(X2)^iPr_2\}_2]$: X1 = S, X2 = Se (**1**), X1 = X2 = S (**2**), and X1 = X2 = Se (**3**) have been successfully used as single-source precursors (SSPs) to deposit thin films of nickel sulfide, selenide or phosphide; the material deposited depended on both temperature and method used for the deposition. Aerosol-assisted (AA) chemical vapour deposition (CVD) and low-pressure (LP) CVD were used. The as-deposited films were characterised by X-ray diffraction (XRD), scanning electron microscopy (SEM), energy dispersive X-ray spectroscopy (EDX) and X-ray photoelectron spectroscopy (XPS). A variety of phases including: Ni_2P, $Ni_{0.85}Se$ and $NiS_{1.03}$ were deposited under different conditions. The mechanism of decomposition to the phosphide, selenide, or sulfide was studied by pyrolysis gas chromatography mass spectrometry (Py-GC-MS) and modelled by density functional theory (DFT).

Introduction

Many potentially useful and technologically important films have been grown by metal–organic chemical vapour deposition (MOCVD).[1,2] The term was coined by Manasevit to describe processes for the deposition of group 12 or 13 metal chalcogenides or pnictides, II/VI (12/16) or III/V (13/15) materials.[1] The typical sources used in early studies were hydrides and alkyls which are often highly reactive (*e.g.* pyrophoric), toxic, air-sensitive and susceptible to pre-reaction in the vapour phase. Some of these issues can be overcome by the use of single-source precursors (SSPs), which provide the requisite elements for the deposition of the material in a single molecule.

Chalcogenide films are of interest for large area photodiode arrays, photoconductors, sensors, solar cells, optical storage discs and fibres.[3] We have developed a range of SSPs for such thin films.[4] The diselenoimidodiphosphinato complexes of the type $[M\{(SePPh_2)_2N\}_2]$ (M = Cd, Zn) have been used for the deposition of CdSe or ZnSe thin films.[5] The isopropyl group gives better volatility than the phenyl group, leads to the facile deposition of a variety of metal sulfide or selenide thin films.[6] In addition, we have also reported the formation of group 11 and 12 metal telluride films from the corresponding ditelluroimidodiphosphinato complexes.[7] Apart from our CVD work using thioseleno-$[Ni\{^iPr_2P(S)NP(Se)^iPr_2\}_2]$[8] (**1**) and selenotelluro-$[Ni\{^iPr_2P(Se)NP(Te)^iPr_2\}_2]$[9] precursors, there are no other reports on using the mixed donor group dichalcogenoimidodiphosphinato complexes as precursors.

The idea inspiring the design of (**1**) was to establish a new route to ternary MSSe phases such as nickel sulfo-selenide ($NiS_{2-x}Se_x$) which can undergo a Mott-Hubbard metal-insulator transition dependent on the selenium content.[10] Serendipitously[8] our failure to achieve this goal showed that (**1**) in low-pressure (LP)CVD gave nickel phosphide films at higher substrate temperatures (475–425 °C) and nickel selenide films at lower substrate temperatures (400 and 375 °C) (the delivery temperature was kept constant at 300 °C). A heterostructured film of $Ni_{0.85}Se/Ni_2P$ was deposited by changing the growth temperature during a single deposition.[8] This result provided the impetus for the study of corresponding dithio (**2**) and diseleno (**3**) precursors, with the objective of understanding the various factors controlling this interesting process.

The sulfides, selenides and phosphides of nickel are semiconductors potentially useful as electrodes in photoelectrochemical storage devices.[11–13] Nickel sulfide and nickel selenide are p-type semiconductors with band gaps of 0.3 eV and 2.0 eV respectively, whereas nickel phosphide is an n-type semiconductor with a band gap of 1.0 eV. Nickel sulfide undergoes a phase transition from paramagnetic metal to antiferromagnetic semiconductor at 265 K; the mechanism of this change is still unclear and under investigation.[14] Nickel sulfide is a potential cathode material for rechargeable lithium batteries[15] and is also used as a hydrodesulfurisation catalyst.[16] It is considered as an "Achilles heel" in toughened glass, since it is responsible for glass cancer or spontaneous glass fracture. The phase diagram for the Ni–S

[a]*The School of Chemistry and the School of Materials, The University of Manchester, Oxford Road, Manchester, UK M13 9PL. E-mail: paul.obrien@manchester.ac.uk; Fax: +44 161 2754598; Tel: +44 161 2754653*
[b]*The School of Chemistry, The University of Manchester, Oxford Road, Manchester, UK M13 9PL. E-mail: neil.burton@manchester.ac.uk*
[c]*School of Earth, Atmospheric and Environmental Sciences and Williamson Research Centre for Molecular Environmental Science, The University of Manchester, Oxford Road, Manchester, UK M13 9PL*

† Electronic supplementary information (ESI) available: TGA of precursors (**1**), (**2**) and (**3**); XRD of nickel selenide films deposited from (**1**) at 240 sccm, nickel sulfide films deposited from (**2**) at 200 sccm at 425 and 475 °C by AACVD; XPS spectra of Ni2p and S2p; XRD of nickel selenide films deposited from (**3**) by LPCVD; Precursor structure, model used in the calculations and additional computational data for the precursors. See DOI: 10.1039/c002928a

 This journal is © The Royal Society of Chemistry 2010

system indicates NiS_2 (pyrite) and Ni_3S_4 (spinel) for the sulfur-rich part of the system. For the nickel-rich part of the diagram, multiple phases such as NiS, Ni_3S_2, Ni_7S_6 and Ni_9S_8 exist and are associated with the glass fracture except the Ni_3S_2 phase.[17,18]

Nickel sulfide films have been prepared by solution deposition on glass[19] or polymer substrates,[20] electrodeposition,[12] successive ionic layer adsorption and reaction,[21] laser ablation,[22] hydrothermal[23] and soft solution-processing[24] methods. There are limited reports on the growth of nickel sulfide films by CVD using single-source precursors. Zink *et al.* have reported on the laser-driven photochemical and thermal CVD of NiS from bis(*O*-isopropylxanthate)nickel(II) precursor.[25] Nomura and co-workers studied the growth of $NiS_{1.03}$ from $[Ni(S_2CNEt_2)_2]$ on Si(111) substrates by LPCVD.[26] Earlier, we have reported the deposition of nickel sulfide films from dithiocarbamato compounds of the type $[Ni(S_2CNRR')_2]$ (R, R′ = Et_2; Me,Et; Me,^{n}Bu or Me,^{n}Hex), by LP-[27] and aerosol-assisted (AA) CVD;[28] and from xanthate compounds of the type $[Ni(S_2COR)_2]$ (R = Et or ^{i}Pr) by AACVD.[29] Recently, Molloy and co-workers deposited NiS films from the bis-pyridine adducts of nickel bis(*O*-n-butylxanthate) by AACVD.[30]

Nickel selenide films have been prepared by solution growth,[19] electrodeposition[31] and by reactive diffusion methods.[32] The phase diagram of Ni–Se alloys indicates three homogenous and stable phases at room temperature, Ni_3Se_2, $Ni_{1-x}Se$ and $NiSe_2$.[33] Bochmann *et al.* used $[Ni\{^tBu_2P(Se)NR\}_2]$ (R = ^{i}Pr or cyclo-C_6H_{11}) to deposit nickel selenide films by LPCVD method.[34] We have recently made a comparative study of the influence of the ligand on the deposition of nickel selenide films by AACVD using three different classes of nickel precursors: diselenoimidodiphosphinato $[Ni\{(SeP^iPr_2)_2N\}_2]$ (**3**), diselenophosphinato $[Ni(Se_2P^iPr_2)_2]$ and diselenocarbamato $[Ni(Se_2CNEt_2)_2]$.[35]

There are relatively few reports on the growth of nickel phosphide films apart from our CVD work,[8] but depositions by magnetron sputtering,[36] electrodeposition,[37] solution growth[38] or by the reaction of orthophosphoric acid on a nickel substrate can be noted.[12] In the Ni–P binary phase diagram, Ni_3P, Ni_5P_2, $Ni_{12}P_5$, Ni_2P and Ni_5P_4 phases are obtained in sequence with increasing phosphorus content.[39]

This work presents a comprehensive AACVD and LPCVD study of the dichalcogenoimidodiphosphinato nickel(II) precursors $[Ni\{^iPr_2P(S)NP(Se)^iPr_2\}_2]$[8] (**1**), $[Ni\{(SP^iPr_2)_2N\}_2]$[40] (**2**) and $[Ni\{(SeP^iPr_2)_2N\}_2]$[35] (**3**) which gave nickel sulfide, selenide or phosphide films depending on the deposition temperature. A mechanism is proposed for the formation of the different materials based upon a computational study and pyrolysis gas chromatography mass spectrometry (Py-GC-MS).

Results and discussion

Thermogravimetric analysis (TGA) of the precursors $[Ni\{^iPr_2P(S)NP(Se)^iPr_2\}_2]$ (**1**), $[Ni\{(SP^iPr_2)_2N\}_2]$ (**2**) and $[Ni\{(SeP^iPr_2)_2N\}_2]$ (**3**) indicated a single step decomposition with a rapid weight loss between 302–368 °C, 308–371 °C and 300–353 °C, respectively (N_2 atmosphere at 10 °C min^{-1}). The observed residue (11%) for (**1**) is lower than the calculated residue (18%) for nickel selenide, but matches fairly well the expected residue (11.5%) for nickel phosphide. The observed residue (3%) for (**2**) is lower than the calculated residue (13%) for the Ni and S content or Ni and P (11.5%) content in the precursor. For (**3**), the observed residue (17%) is in fair agreement with the calculated residue (16%) for nickel selenide (Fig. S1, in supporting information†).

Deposition of thin films

AACVD of nickel selenide films from (1) at flow rate of 160 sccm

AACVD from precursor (**1**) $[Ni\{^iPr_2P(S)NP(Se)^iPr_2\}_2]$ was carried out to determine if it can form different products to those observed in the LPCVD process.[8] In AACVD the important parameters are: the concentration of the precursor solution, duration of film growth, the deposition temperature and flow rate. Flow rate and temperature were varied to obtain films of different composition or morphologies; using a constant precursor concentration of 0.01 M and deposition time of 120 min. Films were deposited at temperatures 425 to 525 °C, with argon flow rates of 160 or 240 sccm. The films deposited were uniformly black and non-adherent. Film obtained at 375 °C was too thin to be characterised by XRD. Substrate temperatures below 375 °C were insufficient to cause deposition.

The XRD patterns from the films correspond to hexagonal $Ni_{0.85}Se$ (sederholmite, ICDD 18-0888) at all deposition temperatures (425–525 °C). The high intensity peak is along the (101) direction which is the 100% peak in the ICDD 18-0888 pattern (Fig. 1(a)–(c)). Hexagonal NiSe (ICDD 75-0610) was observed at 2θ: 28.15°. The SEM images revealed that the films were composed of wires covered by granular material (Fig. 2(a)–(c)). No remarkable change was observed in the morphology of the as-deposited films at increased growth temperature. EDX analyses of the film deposited at 425 °C contain nickel and selenium *ca*: 1 : 1 ratio with phosphorus (~22%) and sulfur (3%) impurities. The composition of the as-obtained films at higher temperatures (475 and 525 °C) were in good agreement with the phase observed in XRD [*ca.* 0.85–0.92 : 1 (Ni : Se)] with phosphorus contamination (~15%, 475 °C; ~5%, 525 °C) and no sulfur.

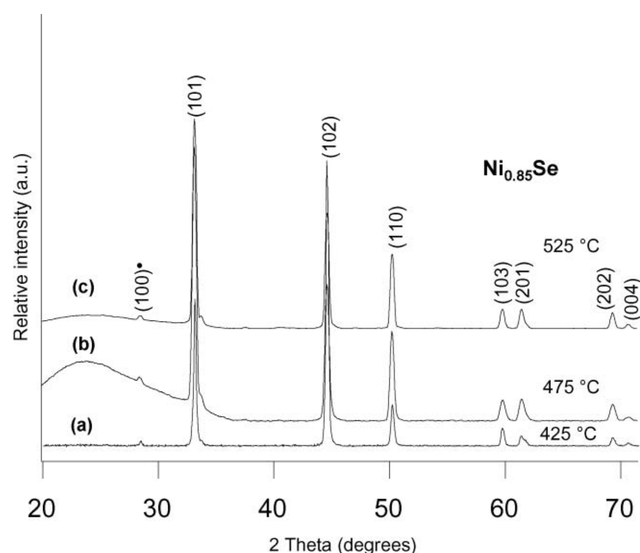

Fig. 1 XRD patterns of nickel selenide ($Ni_{0.85}Se$) films deposited from (**1**) on glass at flow rate of 160 sccm and deposition temperatures of (a) 425 °C, (b) 475 °C and (c) 525 °C, "●" - NiSe peak.

Downloaded by Massachusetts Institute of Technology on 22 October 2011
Published on 01 June 2010 on http://pubs.rsc.org | doi:10.1039/C002928A

Downloaded by Massachusetts Institute of Technology on 22 October 2011
Published on 01 June 2010 on http://pubs.rsc.org | doi:10.1039/C002928A

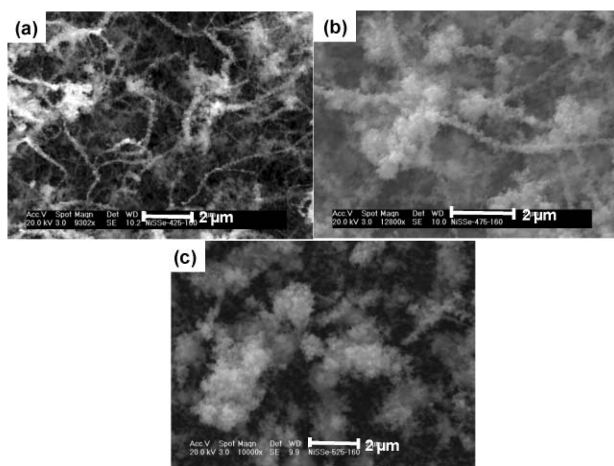

Fig. 2 SEM images of nickel selenide films deposited on glass by AACVD from $[Ni\{^iPr_2P(S)NP(Se)^iPr_2\}_2]$ at a flow rate of 160 sccm and deposition temperatures of (a) 425 °C, (b) 475 °C and (c) 525 °C.

AACVD of nickel selenide and nickel phosphide films from (1) at 240 sccm

The films were deposited at the higher argon flow rate of 240 sccm, the XRD pattern of the as-deposited films at 425 °C and 475 °C could be indexed to a hexagonal $Ni_{0.85}Se$ (ICDD 18-0888) structure. Small peaks for hexagonal Ni_2P (ICDD 74-1385) were observed for the sample grown at 475 °C with 2θ values of 40.81, 47.49 and 54.33° corresponding to (111), (210) and (300) planes along with the characteristic peaks for $Ni_{0.85}Se$ (Fig. S2†).

The higher flow rate resulted in the formation of two different materials at 525 °C: a nickel selenide film on the substrate closer to the inlet of the AACVD reactor and a nickel phosphide film deposited onto the adjacent substrate. The XRD displayed peaks that matched hexagonal $Ni_{0.85}Se$ (Fig. 3(a)). The XRD of the film deposited on the adjacent substrate matched with hexagonal Ni_2P (Fig. 3(b)) but the films were not as crystalline as those of nickel selenide. Traces of hexagonal Ni_5P_4 (ICDD 18-0883) were observed at 2θ values of 32.71 and 49.89° which correspond to the (004) and (006) planes along with the characteristic peaks of Ni_2P.

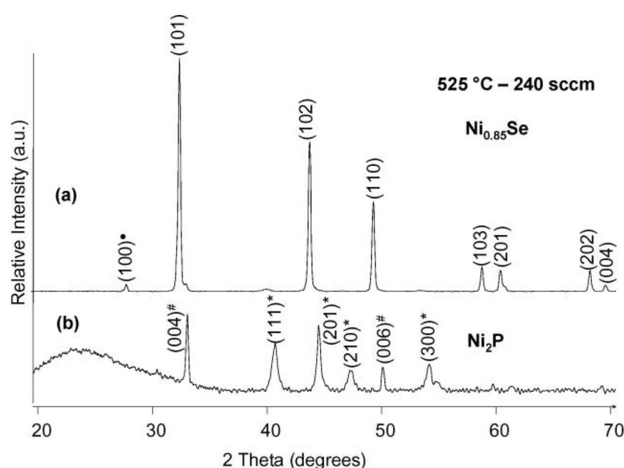

Fig. 3 XRD patterns of (a) nickel selenide ($Ni_{0.85}Se$) and (b) nickel phosphide films (Ni_2P*) deposited on glass from (**1**) at flow rate of 240 sccm and deposition temperature of 525 °C, "#" - Ni_5P_4, "●" - NiSe peak.

The nickel selenide films deposited at 425 °C were composed of wires covered with granular material, whereas at 475 °C convoluted wires were observed above the grains (Fig. 4(a)–(b)). EDX analysis of the film obtained at 425 °C confirms the presence of Ni and Se in *ca.* 0.87 : 1 ratio with phosphorus (~12%) and sulfur (~2%) contamination. The film composition varies at 475 °C to *ca.* 1 : 1 ratio (Ni : Se) with 18% P contamination and no sulfur. The increase in nickel and phosphorus content may be due to the presence of traces of nickel phosphide indicated by XRD (Fig. S2†).

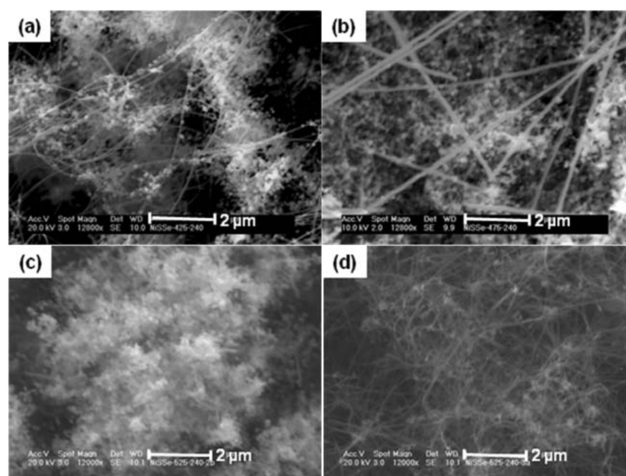

Fig. 4 SEM images of nickel selenide films deposited on glass by AACVD from $[Ni\{^iPr_2P(S)NP(Se)^iPr_2\}_2]$ at flow rate of 240 sccm and deposition temperatures of (a) 425 °C, (b) 475 °C, (c) nickel selenide and (d) nickel phosphide films deposited at 525 °C.

The SEM of as-deposited films at 525 °C show granular nickel selenide and inter-linked nickel phosphide nanowires (Fig. 4(c)–(d)). EDX analysis show nickel rich films with the elemental composition of *ca.* 1.06 : 1 (Ni : Se) with ~6% phosphorus contamination. The Ni_2P wires were composed of nickel and phosphorus in *ca.* 1.2 : 1 with no contamination of selenium. Thus, the growth parameters, higher temperature (525 °C) and higher flow rate (240 sccm) were critical and resulted in the deposition of two different materials; $Ni_{0.85}Se$ and Ni_2P depending upon the position of the substrate inside the reactor. They also influence the composition, crystallinity and morphology of the films.

LPCVD of nickel phosphide and nickel selenide films from (1) at precursor temperature (T_{prec}) 275 °C

In this experiment, the precursor was heated at 275 °C and the substrate temperature was varied from 475–375 °C in 25 °C steps; similar to the regime used in our earlier work but in which the precursor was heated at 300 °C.[8] The lower precursor temperatures should decrease the rate of transport of the precursor to the substrate. The XRD of the as-deposited film showed hexagonal Ni_2P (ICDD 74-1385) at substrate temperatures of 475 °C (Fig. 5(a)), 450, 425 and 400 °C (Fig. 5(b)). Traces of hexagonal nickel selenide ($Ni_{0.85}Se$, ICDD 18-0888) was also observed at 400 °C (2θ: 33.29, 50.56, 60.35, 61.87 and 69.73°).

 This journal is © The Royal Society of Chemistry 2010

Published on 01 June 2010 on http://pubs.rsc.org | doi:10.1039/C002928A
Downloaded by Massachusetts Institute of Technology on 22 October 2011

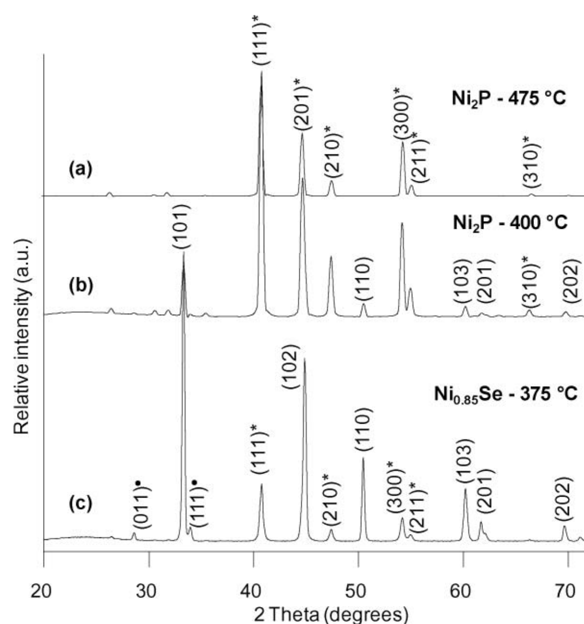

Fig. 5 XRD patterns of nickel phosphide (Ni_2P*) films deposited on glass from (**1**) at substrate temperatures of (a) 475 °C, (b) 400 °C and nickel selenide ($Ni_{0.85}Se$) films deposited at substrate temperature of (c) 375 °C; T_{prec} = 275 °C for all cases. "●" - $NiSe_2$ peaks.

At 375 °C, hexagonal $Ni_{0.85}Se$ was observed with traces of $NiSe_2$ (ICDD 18-0886, 2θ: 28.58 and 33.72°). Peaks observed at 2θ values of 40.87, 47.56, 54.31 and 55.10° correspond to hexagonal Ni_2P (Fig. 5(c)).

The SEM shows varied morphology: cross-linked wires (475 °C), acicular structures (450 °C), stacked rods (425 °C) and stacked wires (400 °C) for the nickel phosphide films (Fig. 6(a)–(d)). The as-deposited nickel selenide film (375 °C) has feather-like morphology (Fig. 6(e)). EDX investigation of the film grown at 475 °C was rich in nickel (79%) with 21% phosphorus. The composition of the Ni_2P films deposited at 450 and 425 °C were in close agreement with the phase observed in XRD with elemental ratio of *ca.* 1.9 : 1 (Ni : P). As-obtained phosphide film at 400 °C contain 60% nickel, 32% phosphorus and 8% selenium due to the formation of trace amounts of nickel selenide as indicated in the XRD. The nickel selenide film grown at 375 °C was composed of 51% nickel, 39% selenium and 10% phosphorus due to the presence of traces of nickel phosphide in the deposited film. Thus, the lowering of the precursor temperature resulted in the deposition of nickel phosphide films at 475–400 °C and nickel selenide film only at 375 °C.

XPS of nickel phosphide film showed a $Ni2p_{3/2}$ peak at 853.5 eV along with a satellite at 860.4 eV which is consistent with pure nickel phosphide.[41] In the case of the P2p, two doublets appear at 129.9 and 133.5 eV, corresponding to phosphide and phosphate, respectively.[42] Two additional peaks for selenium were also observed at 54 eV (for bound selenium) and 55 eV (for unbound selenium). For nickel selenide film, main $Ni2p_{3/2}$ peak appeared at 853 eV and a satellite at 857.9 eV which is in good agreement with the literature values.[43] The Se3d peak at 53.9 eV corresponds to metallic selenide. The presence of the O1s peaks in both films indicated that oxidation of films takes place after exposure to the atmosphere.

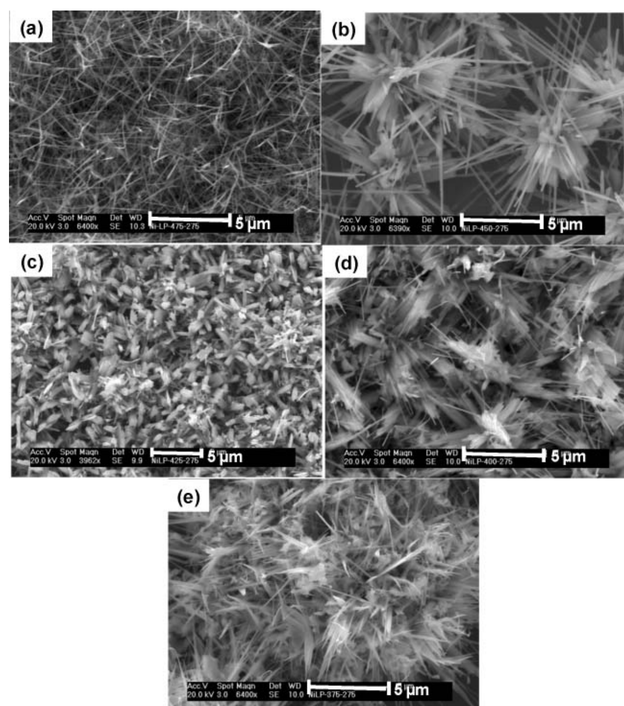

Fig. 6 SEM images of nickel phosphide films deposited on glass by LPCVD from $[Ni\{^iPr_2P(S)NP(Se)^iPr_2\}_2]$ at substrate temperatures of (a) 475 °C, (b) 450 °C, (c) 425 °C (d) 400 °C and nickel selenide film deposited at substrate temperature of (e) 375 °C, T_{prec} = 275 °C for all cases.

AACVD of nickel sulfide films from (2) at 140 sccm

AACVD from $[Ni\{(SP^iPr_2)_2N\}_2]$ (**2**) yielded black films at 425 to 525 °C at argon flow rate of 140 sccm. No deposition was observed below 425 °C. The deposition time for each run was 90 min. The XRD studies of the films obtained at 425, 475 and 525 °C, (Fig. 7(a)–(c)) showed the formation of a mixture of hexagonal $NiS_{1.03}$ (ICDD 02-1273) and orthorhombic Ni_9S_8 (ICDD 22-1193). The films deposited at 425 and 475 °C contains Ni_9S_8 as the major phase; whereas $NiS_{1.03}$ is the predominant phase for the film deposited at 525 °C. As-deposited film at 475 °C showed

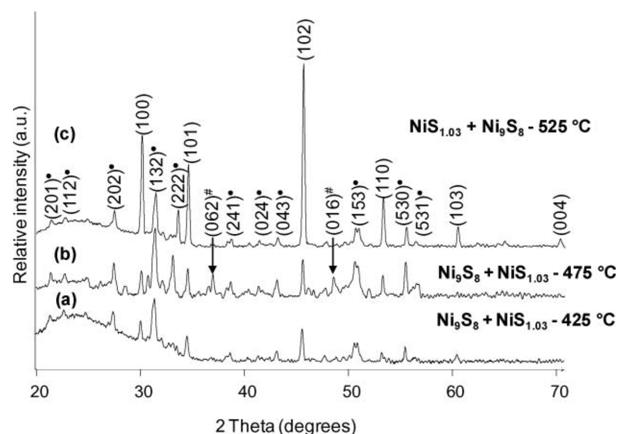

Fig. 7 XRD patterns of nickel sulfide ($NiS_{1.03}$) films deposited on glass from (**2**) at flow rate of 140 sccm and deposition temperatures of (a) 425 °C, (b) 475 °C and (c) 525 °C, "●" - Ni_9S_8, "#" - Ni_7S_6 peaks.

orthorhombic Ni_7S_6 (ICDD 24-1021) at 2θ values of 36.86 and 48.59° in addition to the characteristic peaks for Ni_9S_8 and $NiS_{1.03}$ phases (Fig. 7(b)).

The SEM images of the films deposited at 425 °C were composed of intertwined wires (Fig. 8(a)) whereas at 475 and 525 °C stacked rods and wires can be noted (Fig. 8(b)–(c)). Altogether there is no appreciable change in the morphology of the films with the variation of deposition temperatures. The EDX analysis of the as-prepared films grown at 425 and 475 °C were nickel rich [*ca.* 1.15–1.20 : 1 (Ni : S)] with phosphorus impurities (~7% at 425 °C and ~3% at 475 °C). The film obtained at 525 °C was highly deficient in sulfur with elemental composition of *ca.* 1.39 : 1 (Ni : S) and 10% phosphorus contamination.

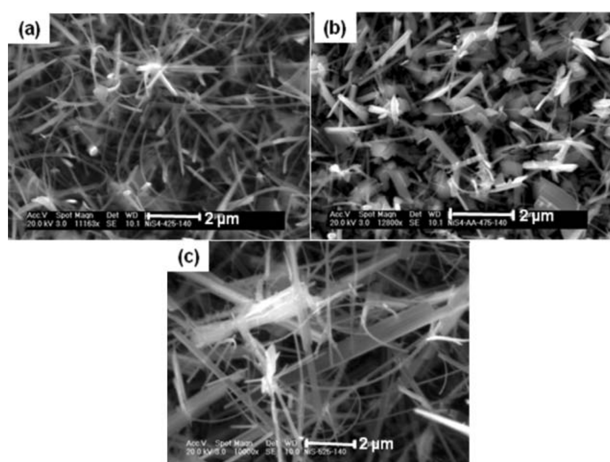

Fig. 8 SEM images of nickel sulfide films deposited on glass by AACVD from $[Ni\{(SP^iPr_2)_2N\}_2]$ at flow rate of 140 sccm and growth temperatures of (a) 425 °C, (b) 475 °C and (c) 525 °C.

AACVD of nickel sulfide films from (2) at 200 sccm

The XRD patterns of the films deposited at 425 and 475 °C showed a mixture of two phases, predominantly hexagonal $NiS_{1.03}$ (ICDD 02-1273) with traces of orthorhombic Ni_7S_6 (ICDD 24-1021). The high intensity peak for the films deposited at 425 and 475 °C is along (102) direction of $NiS_{1.03}$ phase (Fig. S3†). Traces of hexagonal Ni_2P (ICDD 74-1385) peaks were detected at 2θ values of 40.85, 44.78 and 54.28° for the film deposited at 475 °C. These results are different to the films deposited at 425 and 475 °C at 140 sccm where the Ni_9S_8 phase was predominantly deposited.

The XRD analysis of the films deposited at 525 °C, 200 sccm revealed the formation of two different materials which were not observed at 140 sccm; nickel sulfide (Fig. 9(a)) on the glass substrate closer to the precursor inlet and nickel phosphide film (Fig. 9(b)) on the adjacent substrate. The nickel sulfide film is composed of two phases, the major phase being hexagonal $NiS_{1.03}$. The minor phase is orthorhombic Ni_9S_8 (ICDD 22-1193) with 2θ values at 27.25, 31.43, 50.71 and 55.56°. Hexagonal Ni_2P (ICDD 74-1385) film was observed on the substrate kept at the middle part of the AACVD reactor.

The films were composed of wires and irregular crystallites at 425 °C and a mixture of individual and stacked wires at 475 °C (Fig. 10(a)–(b)). EDX analysis of the film deposited at 425 °C show the presence of nickel and sulfur in *ca.* 1.09 : 1 stoichiometry

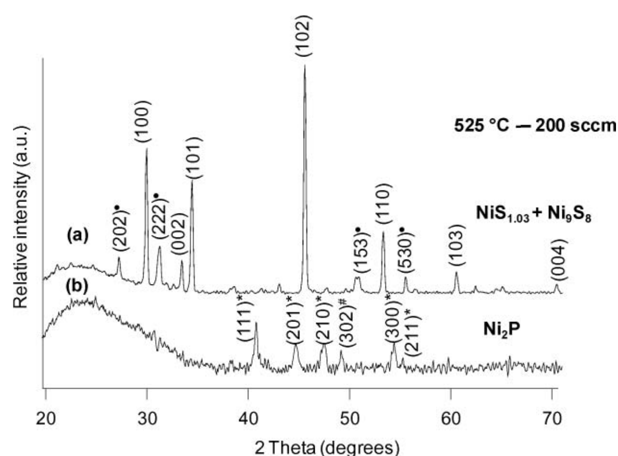

Fig. 9 XRD patterns of (a) nickel sulfide ($NiS_{1.03}$) and (b) nickel phosphide (Ni_2P*) films deposited on glass from (**2**) at flow rate of 200 sccm and deposition temperature of 525 °C, "#" - Ni_5P_4, "●"- Ni_9S_8 peaks.

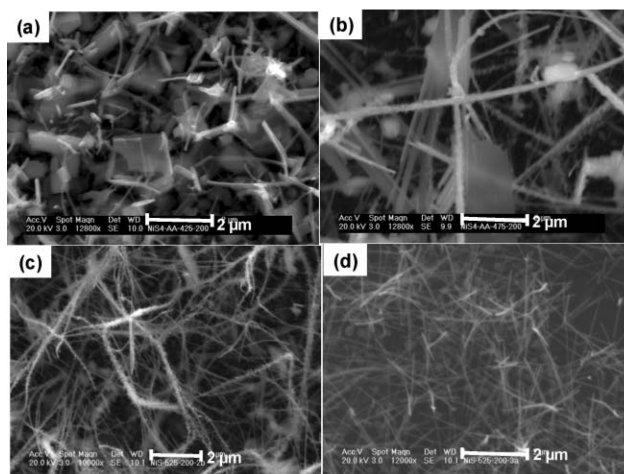

Fig. 10 SEM images of nickel sulfide films deposited on glass by AACVD from $[Ni\{(SP^iPr_2)_2N\}_2]$ at flow rate of 200 sccm and growth temperatures of (a) 425 °C, (b) 475 °C, (c) nickel sulfide and (d) nickel phosphide films deposited at 525 °C.

with 3% phosphorus, whereas for the film deposited at 475 °C the composition changes to *ca.* 1.45 : 1 (Ni : S) with 10% phosphorus contamination. Increase in nickel and phosphorus content may be due to the formation of nickel phosphide as shown in Fig. S3.†

The SEM of the films deposited at 525 °C revealed the formation nickel sulfide wires coated with granular material (Fig. 10(c)) and randomly overlapped nickel phosphide wires (Fig. 10(d)). The nickel sulfide wires was sulfur deficient (29%), with nickel (54%), and 17% phosphorus contamination, whereas phosphide wires was rich in phosphorus (65%) with nickel (35%) and no detectable sulfur.

The XPS spectrum of the film deposited at 525 °C is shown in Fig. S4,† the Ni2p spectrum indicated two different types of Ni species. In both cases, two contributions of the Ni2p appear. The $Ni2p_{3/2}$ peak at 853 eV with a broad shake-up satellite at about 860 eV is consistent with NiS phase of the film.[44] Other $Ni2p_{3/2}$ peak at 855.8 eV with a 861 eV satellite indicates the presence of oxidized/hydrolysed Ni species such as an oxide. The presence of

Downloaded by Massachusetts Institute of Technology on 22 October 2011
Published on 01 June 2010 on http://pubs.rsc.org | doi:10.1039/C002928A

This journal is © The Royal Society of Chemistry 2010

such a material is further confirmed by the appearance of O1s peak at 531 eV. The S2p spectrum presented in Fig. S5† shows that sulfur exists in three forms. The peak at 162 eV corresponds to sulfur in NiS, 163 eV to elemental sulfur and 165 eV to sulfate.[45] The band at low binding energy value, 130 eV, is assigned to phosphorus in the form of Ni_2P; another one at 133.5 eV is a typical of phosphite species.

LPCVD of nickel phosphide films from (2) at T_{prec} = 300 °C

Film deposition from $[Ni\{(SP^iPr_2)_2N\}_2]$ was carried out at substrate temperatures (475 to 400 °C) and at precursor temperature of 300 °C for 60 min. The XRD pattern of the as-deposited samples at substrate temperatures of 475 and 450 °C (Fig. 11(a)–(b)) matched with the standard pattern for hexagonal Ni_2P (ICDD 74-1385) whereas at 425 °C, the XRD (Fig. 11(c)) showed traces of hexagonal nickel sulfide ($NiS_{1.03}$, ICDD 02-1273) peaks at 2θ values of 34.21, 45.86 and 53.27° apart from the characteristic peaks for Ni_2P. No deposition was observed at 400 °C or below. The high intense peak correspond to the (111) plane at all substrate temperatures which coincides to the 100% peak reported for Ni_2P in the X-ray diffraction database.

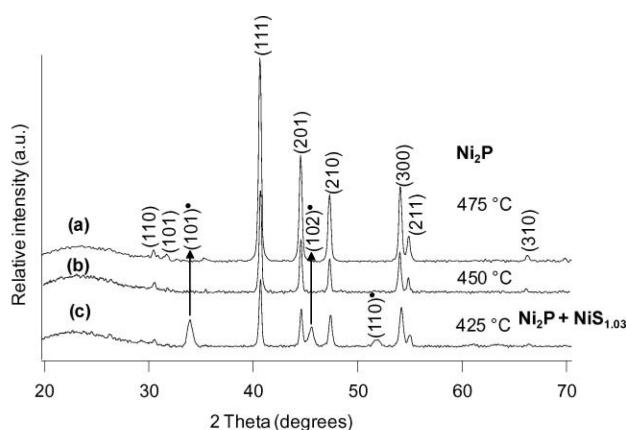

Fig. 11 XRD patterns of nickel phosphide (Ni_2P) films deposited on glass from (**2**) at substrate temperatures of (a) 475 °C, (b) 450 °C and (c) 425 °C; T_{prec} = 300 °C for all cases. "●" - $NiS_{1.03}$ peaks.

The SEM analysis of the nickel phosphide films deposited at 475 °C revealed two types of morphologies; flowers and aggregates of randomly shaped particles (Fig. 12(a)). EDX measurements on the flowers gave the composition as *ca.* 1.95 : 1 (Ni : P), with 3% sulfur, whereas the particles contain nickel and phosphorus in *ca.* 1.4 : 1 ratio. The films deposited at 450 °C (Fig. 12(b)) contain bundles of wires with nickel and phosphorus in *ca.* 1.6 : 1 stoichiometry and traces of sulfur (3%). Interlinked wires of nickel phosphide deposited at 425 °C (Fig. 12(c)), were phosphorus rich (52%) with nickel (42%), contaminated with 6% sulfur.

Influence of precursor temperature (275 °C) on the growth of a mixture of nickel phosphide and nickel sulfide films from (2) by LPCVD

When the precursor temperature was decreased to 275 °C, XRD of the as-deposited films at substrate temperature 475 °C (Fig. 13(a)) exhibited peaks for Ni_2P (ICDD 74-1385) with traces of hexagonal NiS (ICDD 77-1624) and cubic Ni_3S_4 (ICDD 76-1813) phases.

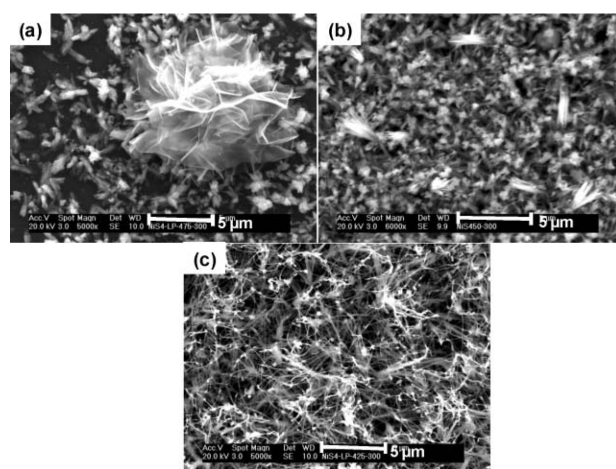

Fig. 12 SEM images of nickel phosphide films deposited on glass by LPCVD from $[Ni\{(SP^iPr_2)_2N\}_2]$ at substrate temperatures of (a) 475 °C, (b) 450 °C and (c) 425 °C, T_{prec} = 300 °C for all cases.

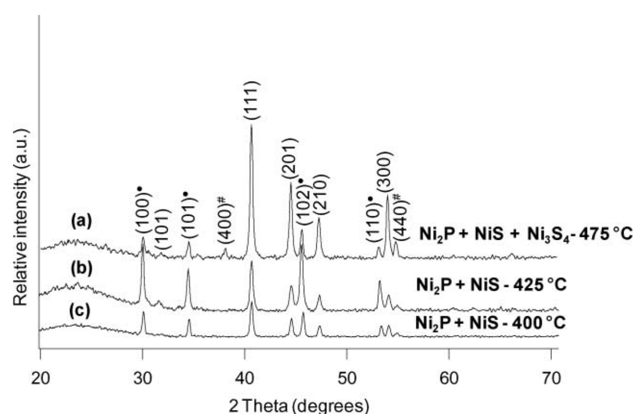

Fig. 13 XRD patterns of nickel phosphide (Ni_2P) and nickel sulfide ($NiS^{\bullet}$) films deposited on glass from (**2**) at substrate temperature of (a) 475 °C, (b) 425 °C and (c) 400 °C; T_{prec} = 275 °C, "#" - Ni_3S_4 peaks.

At lower substrate temperatures [450, 425 °C Fig. 13(b)], the amount of Ni_2P was lowered which is expressed as a reduction in the intensity of the (111) peak and increase in the relative intensities of the NiS peaks at 2θ values of 30.07, 34.53, 45.77 and 53.25° corresponding to (100), (101), (102) and (110) planes respectively. At 400 °C (Fig. 13(c)), the intensity of both NiS and Ni_2P peaks were reduced compared to 450 and 425 °C due to the poor crystallinity of the film because of the low substrate temperature. No deposition was noted at 375 °C.

The SEM images revealed that the nickel phosphide film deposited at 475 °C consist of bundles of wires (Fig. 14(a)) whereas at 450 °C, phosphide plates and sulfide clusters were fused together (Fig. 14(b)). Similarly at 425 °C (Fig. 14(c)), two different morphologies were observed; the flakes correspond to nickel phosphide, and the aggregates of spherical particles correspond to nickel sulfide. The nickel phosphide plates were sandwiched between NiS spongy features at 400 °C (Fig. 14(d)). EDX analysis of the film grown at 475 °C indicate the presence of nickel and phosphorus in *ca.* 1.85 : 1 ratio contaminated with 10% sulfur due to the presence of nickel sulfide. The nickel sulfide particles obtained at 450–400 °C were nickel rich with elemental composition of *ca.* 1.2–1.4 : 1 (Ni : S) ratio whereas the phosphide

Downloaded by Massachusetts Institute of Technology on 22 October 2011
Published on 01 June 2010 on http://pubs.rsc.org | doi:10.1039/C002928A

Downloaded by Massachusetts Institute of Technology on 22 October 2011
Published on 01 June 2010 on http://pubs.rsc.org | doi:10.1039/C002928A

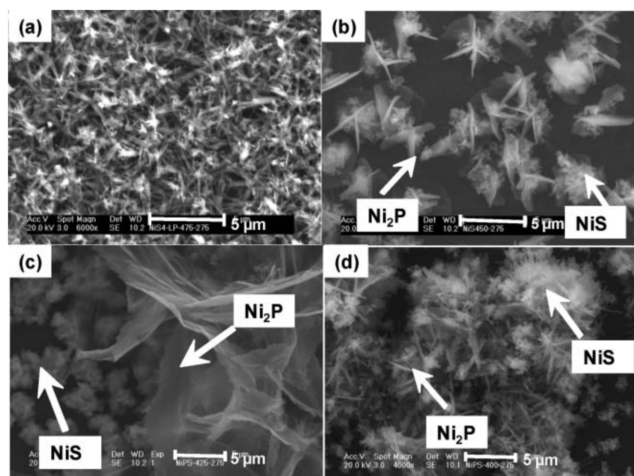

Fig. 14 SEM images of nickel phosphide and nickel sulfide films deposited on glass by LPCVD from $[Ni\{(SP^iPr_2)_2N\}_2]$ at substrate temperature of (a) 475 °C, (b) 450 °C, (c) 425 °C and (d) 400 °C; T_{prec} = 275 °C for all cases.

particles were found to be rich in phosphorus, with elemental ratios of *ca.* 1 : 1.8–2.1 (Ni : P). The visibility of the glass surface infers poor coverage of the film on the surface.

AA- and LP-CVD of nickel selenide films from (3)

We have previously reported the AACVD of nickel selenide films ($Ni_{0.85}Se$) from $[Ni\{(SeP^iPr_2)_2N\}_2]$ (**3**) at deposition temperatures of 400–500 °C at the argon flow rate of 140 sccm.[35] AACVD of (**3**) was now carried out at the higher flow rate of 200 sccm to study its effect on film composition and morphology. The increase in flow rate did not affect the film composition; the as-deposited material was found to be hexagonal $Ni_{0.85}Se$ (ICDD 18-888) by XRD at the temperatures of 425, 475 and 500 °C. The high intense peak is along (101) direction for all deposition temperatures. The SEM studies revealed that the films comprise mixtures of fibrous wires and granular material (Fig. 15(a)–(c)). Granular morphologies were observed to predominate at higher temperatures, whilst lower temperatures gave rise to more fibrous wires. EDX measurements

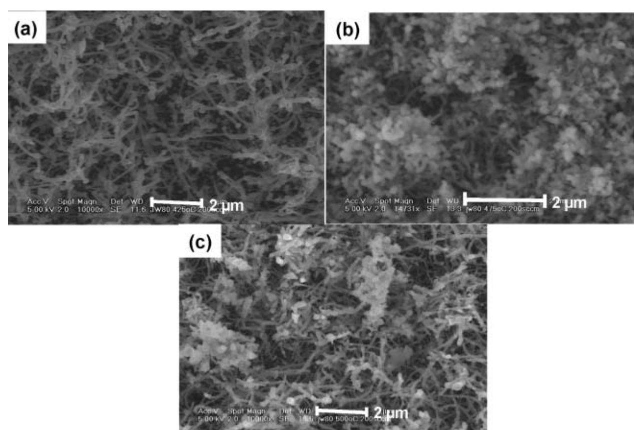

Fig. 15 SEM images of nickel selenide films deposited on glass by AACVD from $[Ni\{(SeP^iPr_2)_2N\}_2]$ at flow rate of 200 sccm and growth temperatures of (a) 425 °C, (b) 475 °C and (c) 500 °C.

confirm that the films comprises of Ni and Se in *ca.* 1 : 1 ratio, in close agreement with the phase observed in the XRD studies.

LPCVD from (**3**) gave smooth grey films at substrate temperatures between 400–475 °C and precursor temperatures of 300 and 275 °C. Whilst film growth was noted across these temperature ranges, the optimal conditions, in terms of film thickness and crystallinity, proved to be at T_{subs} = 425 °C and T_{prec} = 300 and 275 °C. The XRD analysis confirmed that the deposited material was hexagonal $Ni_{0.85}Se$ (ICDD 18-888), with the 100% peak correlating to the (101) reflection as observed in the AACVD studies. It is apparent from the XRD data that the higher precursor temperature (300 °C) leads to improved crystallinity (Fig. S6†).

The SEM analysis showed that the film deposited at T_{prec} = 300 °C comprises granular material, whilst at lower T_{prec} (275 °C) leads to corrugated platelets (Fig. 16(a)–(b)). The films were shown by EDX to be selenium rich, with elemental ratio of *ca.* 0.8 : 1 (Ni : Se) with 5% phosphorus contamination.

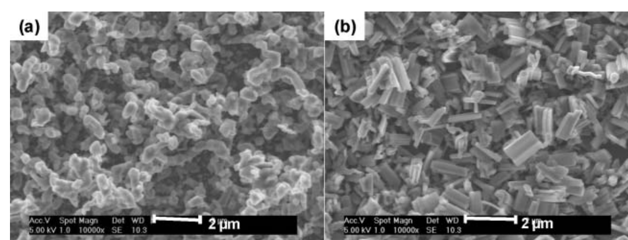

Fig. 16 SEM images of nickel selenide films deposited on glass by LPCVD from $[Ni\{(SeP^iPr_2)_2N\}_2]$ at substrate temperature of 425 °C and T_{prec} (a) 300 °C and (b) 275 °C.

Mechanistic studies by Py-GC-MS and computational DFT methods

The various products obtained by LPCVD and AACVD techniques at different temperatures from $[Ni\{^iPr_2P(S)NP(Se)^iPr_2\}_2]$ (**1**), $[Ni\{(SP^iPr_2)_2N\}_2]$ (**2**) and $[Ni\{(SeP^iPr_2)_2N\}_2]$ (**3**) are represented in Fig. 17 and 18, respectively. There is no direct bond between nickel and phosphorous atoms in any of these precursors.

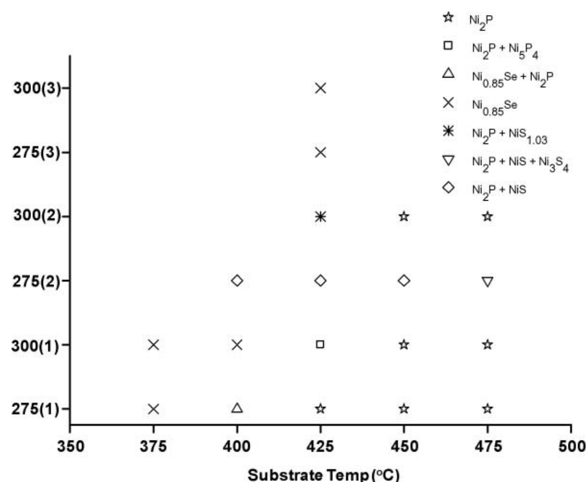

Fig. 17 LPCVD results of compounds given as a function of their precursor and substrate temperatures (°C). Compounds are referenced in brackets on *y* axis. "+" denotes products on the same substrate.

This journal is © The Royal Society of Chemistry 2010

Published on 01 June 2010 on http://pubs.rsc.org | doi:10.1039/C002928A
Downloaded by Massachusetts Institute of Technology on 22 October 2011

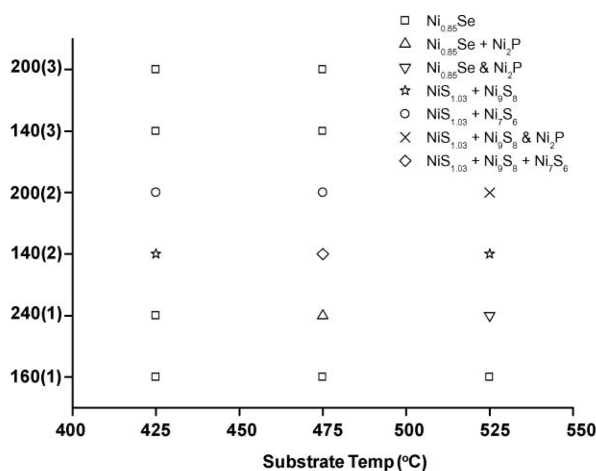

Fig. 18 AACVD results of compounds given as a function of their argon flow rate (sccm) and substrate temperature. Compounds are referenced in brackets on *y* axis. "+" denotes products on the same substrate, "&" denotes products on the different substrate.

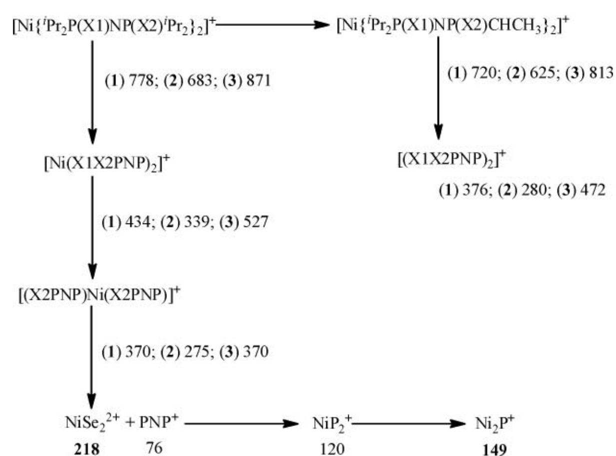

Scheme 1 Plausible decomposition mechanism for $[Ni\{^iPr_2P(X1)NP(X2)^iPr_2\}_2]$ [X1 = S, X2 = Se (**1**); X1 = X2 = S (**2**); X1 = X2 = Se (**3**)] from pyrolysis GC-MS and APCI studies, showing the main fragments observed.

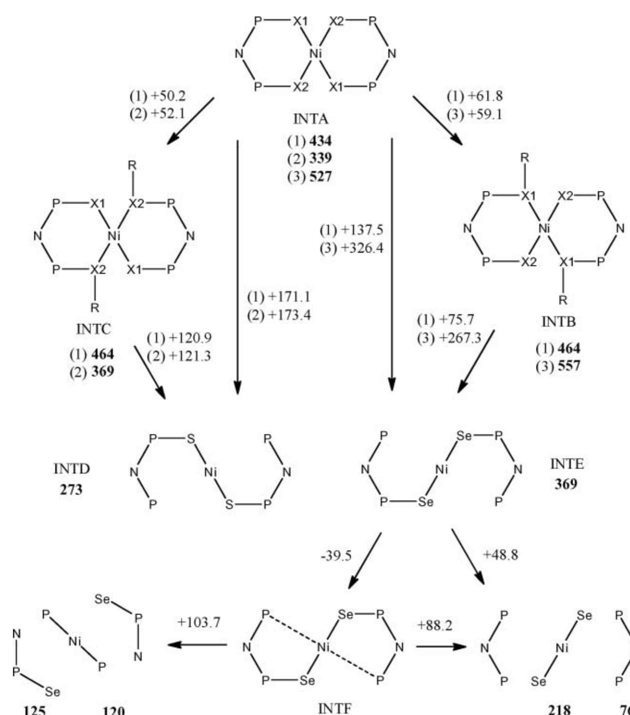

Fig. 19 Illustrative fragmentation mechanism and computed reaction energies (kcal mol^{-1}) for precursors $[Ni\{^iPr_2P(X1)NP(X2)^iPr_2\}_2]$ [X1 = S, X2 = Se (**1**); X1 = X2 = S (**2**); X1 = X2 = Se (**3**)]. Corresponding m/z values observed in the pyrolysis GC-MS experiment are given in bold. The reaction energies are tabulated in Table S1† in the supporting information.

However CVD from (**1**) and (**2**) gave nickel phosphide, selenide or sulfide films, whereas (**3**) gave only nickel selenide films. In addition, CVD from $[M\{(SePR_2)_2N\}_2]$, (M = Zn, Cd, Pb; R = Ph or ^iPr)[5,6a,6b] deposited only metal selenide films. An understanding of the electronic structure of these compounds might explain the formation of nickel phosphide or nickel selenide films from an individual system. In order to study and understand the factors controlling the materials formed in these systems, we have employed Py-GC-MS and density functional theory (DFT) computational methods.

Py-GC-MS is a useful technique in this context since the conditions under which precursor decomposition occur in the instrument are quite similar to the LPCVD process; although clearly only the relatively stable charged fragments will be observed in Py-GC-MS. Density functional theory is a useful and accurate computational method for evaluating the reaction energetics and has proven particularly successful for the study of transition metal complexes and the mechanisms of their reactions.[46] Computational reaction or dissociation energies are presented in order to support the mechanistic arguments based on the Py-GC-MS studies. The DFT method has been used to assess the thermodynamic preferences of the various potential mechanistic steps in order to discern any clear preferences for the observed products. Although many of the general steps shown in Scheme 1 may involve quite detailed and complex reaction mechanisms, we are mindful that a full understanding of the process would ultimately require consideration of each detailed kinetic steps involved. However, to illustrate the main mechanistic preferences and experimental observations in this system, the analysis has been simplified by consideration of model Gibbs reaction energies between the key dissociation products, shown in Fig. 19.

In Scheme 1, a plausible decomposition mechanism is presented for the precursors **1**, **2** and **3**, summarising the main intermediates and products. Each intermediate species can be rationalised through the observation of a corresponding fragment in the pyrolysis MS experiment and each species in Scheme 1 is presented with the m/z value corresponding to the fragment, if observed in one of the Py-GC-MS experiments.

The proposed mechanism involves some common decomposition steps for all the precursors. Hence Scheme 1, can be used to explain the deposition of nickel sulfide or selenide or phosphide thin films. The steps are:

1. The elimination of the alkyl side chains.
2. The elimination of S from the intermediates in preference to Se in precursor (**1**); however precursor (**2**) has only sulfur and (**3**) has only selenium.
3. Initial formation of $NiSe_2$ species from the precursors (**1**) and (**3**) and NiS_2 species from precursor (**2**).

Table 1 Selected experimental (Exp) and computed (DFT) bond-lengths (Å) for the precursors and ring opening intermediates of precursors (**1**), (**2**) and (**3**)

	Complex	Level	Ni–S	Ni–Se	P–S	P–Se	P–N	X1-X2
Precursor **1**	$[Ni\{^iPr_2P(S)NP(Se)^iPr_2\}_2]$	Exp[8]	2.27	2.37	2.08	2.15	1.59	—
	$[Ni\{(CH_3)_2P(S)NP(Se)(CH_3)_2\}_2]$	DFT	2.34	2.38	2.05	2.21	1.62	3.85
INTA	$[Ni(SSePNP)_2]$	DFT	2.35	2.40	2.04	2.21	1.61	3.96
INTB	$[Ni(SCH_3SePNP)_2]$	DFT	2.39	2.37	2.30	2.08	1.64	3.90
INTC	$[Ni(SeCH_3SPNP)_2]$	DFT	2.34	2.40	2.14	2.23	1.62	3.92
Precursor **2**	$[Ni\{^iPr_2P(S)NP(S)^iPr_2\}_2]$	Exp[40]	2.28	—	2.03	—	1.59	—
	$[Ni\{(CH_3)_2P(S)NP(S)(CH_3)_2\}_2]$	DFT	2.33	—	2.06	—	1.62	3.89
INTA	$[Ni(S_2PNP)_2]$	DFT	2.33	—	2.04	2.21	1.60	3.90
INTB	$[Ni(SCH_3SPNP)_2]$	DFT	2.37[a] 2.28	—	2.27[a] 2.09	—	1.60	3.74
Precursor **3**	$[Ni\{^iPr_2P(Se)NP(Se)^iPr_2\}_2]$	Exp[35]	—	2.41	—	2.24	1.60	—
	$[Ni\{(CH_3)_2P(Se)NP(Se)(CH_3)_2\}_2]$	DFT	—	2.38	—	2.21	1.62	3.98
INTA	$[Ni(Se_2PNP)_2]$	DFT	—	2.45	—	2.20	1.60	4.06
INTC	$[Ni(SeCH_3SePNP)_2]$	DFT	—	2.39[a] 2.34	—	2.41[a] 2.23	1.60	3.87

[a] Represents the alkylated S and Se in the precursors (**2**) and (**3**). Computational details are described in the supporting information.†

Downloaded by Massachusetts Institute of Technology on 22 October 2011
Published on 01 June 2010 on http://pubs.rsc.org | doi:10.1039/C002928A

4. A secondary decomposition process to form Ni_2P species for (**1**) and (**2**).

In the following section, the above findings will be rationalised utilising a combination of computational and experimental evidence based upon the Gibbs reaction energies for key intermediates (summarised in Fig. 19 and Table S1†) and the precursor structures (Table 1 and Table S2†).

Ring opening - a preference for the formation of nickel selenide over nickel sulfide

In LPCVD from the precursors, the first step is likely to be the *β*-elimination of the ^{i}Pr groups and indeed the dealkylated fragments are noted in the Py-GC-MS studies with m/z values of 434, 339 and 527 for precursors (**1**), (**2**) and (**3**), respectively (pyrolysis temperature 300 °C). Dealkylation is a typical first dissociation step in many pyrolytic reactions and in this case result in considerable reduction of steric hindrance from the ^{i}Pr groups. The minimum energy structures for the precursors and the possible dealkylated intermediates, INTA arising from removal of the alkyl groups of precursors (**1**), (**2**) and (**3**), are presented in Table 1.

We shall now consider two possible fragmentation pathways (Fig. 19) for precursor (**1**) which may arise from pyrolysis of the dealkylated INTA intermediate: the first route involves ring opening *via* breaking of Ni–Se and Se–P bonds in preference to the Ni–S and S–P bonds, and the second route is the analogous pathway involving preferential breakage of the Ni–S and S–P bonds. Precursors (**2**) and (**3**) follow route 1 and route 2 respectively, since they have identical ligands and no alternative route is available.

The most significant aspect of INTA is the similarity of its structure to the corresponding precursors, with little observable change in the calculated ring bond-lengths to those in the parent compound (see Table 1). In the mixed ligand precursor (**1**) INTA, the Ni–Se bond-lengths 2.40 Å, are longer than the Ni–S bond-lengths 2.35 Å, (as in agreement with a difference in ionic radii between Se and S of 0.13 Å) and therefore are likely to be weaker. So the fragmentation would most likely result in preferential dissociation of the Ni–Se bonds ultimately resulting in NiS_2 species and a nickel sulfide film; however, NiS_2 species are not observed in the Py-GC-MS analysis of (**1**) and furthermore the observed nickel selenide films are not contaminated by sulfur.

In an effort to rationalise this observation for precursor (**1**), we consider that the INTA intermediate may readily interact with available alkyl species and the resulting intermediates would be consistent with the observed fragmentation pattern. To illustrate this mechanism, let us consider two possible intermediates, INTB and INTC, where the S and the Se centres of INTA are alkylated respectively. Alkylation of INTA at both centres will be similarly endoergic, with approximately 62 kcal mol^{-1} required to form INTB and 50 kcal mol^{-1} to form INTC. However, subsequent fragmentation of these intermediates, resulting in ring opening and removal of the two SR groups from INTB, would now be considerably more favourable than removal of two SeR groups from INTC. Overall, the reaction energy for removal of two SR groups from INTA *via* INTB is now considerably more favourable, approximately 138 kcal mol^{-1}, compared to 171 kcal mol^{-1} for removal of two SeR groups from INTA *via* INTC. The Ni–Se bond-length, 2.37 Å in INTB, is shorter than the Ni–S bond-length, 2.39 Å, in line with the dissociation of the Ni–S bonds in preference to the Ni–Se bonds. Furthermore, the formation of an INTB like intermediate results in considerably weaker S–P bonds than Se–P bonds, as shown by a lengthening from 2.04 Å and 2.21 Å in INTA to 2.08 Å and 2.30 Å in INTB respectively, thus contributing to a clear fragmentation and release of SR.

Precursors (**2**) and (**3**) contain four sulfur and selenium atoms respectively, and alkylation is possible at all these positions. However in Fig. 19 we consider only one alkylation of each six member ring which leads to either INTC with bond lengths Ni–SR: 2.37 Å and Ni–S: 2.38 Å for precursor (**2**); or INTB with Ni–SeR: 2.39 Å and Ni–Se: 2.34 Å for precursor (**3**). The formation of the dithio-intermediate INTD from precursor (**2**) would require approximately 173 kcal mol^{-1}, a value similar to that of precursor (**1**). Overall these results conclude that formation

 This journal is © The Royal Society of Chemistry 2010

Downloaded by Massachusetts Institute of Technology on 22 October 2011
Published on 01 June 2010 on http://pubs.rsc.org | doi:10.1039/C002928A

of the INTE diseleno-intermediate from the mixed precursor (**1**), and subsequent formation of $NiSe_2$ is in agreement with the Py-GC-MS observations, and is likely to be more favourable than the formation of a dithio-intermediate INTD which would lead to a pure NiS or NiS_2 species.

Precursors for selenide or phosphide deposition

An important aspect of the deposition mechanism is the deposition of nickel selenide film at lower temperatures from precursors, (**1**) and (**3**). We have noted in the previous section that fragmentation associated with the ring opening will favour the generation of $NiSe_2$ products over NiS_2 products. However, there is no clear evidence to suggest that nickel-phosphide intermediates (NiP_2, NiP or Ni_2P) are favoured during the ring opening. Although intermediates formed as a result of recyclisation followed by ring opening to form INTF, which may be slightly thermodynamically favoured (by around 40 kcal mol^{-1}) over the open structure INTE, the Ni–P bonds in INTF are unlikely to be strong enough to result in preferential dissociation of the Ni–Se bonds at this stage. Instead, we favour the fragmentation pathways which form species such as $NiSe_2$ rather than NiP_2 at this stage and indeed $NiSe_2$ fragments are observed during the Py-GC-MS of precursors (**1**) and (**3**), with peaks observed at m/z values of $NiSe_2^+$:218 and $NiSe^+$:138. At lower temperatures (T < 400 °C), it is therefore proposed that the Ni–Se intermediates from the precursors (**1**) and (**3**), can directly lead to the observed $Ni_{0.85}Se$ thin film. Note that for the precursor (**3**) the removal of SeR is considerably less energetically favourable than for precursor (**1**) but only $NiSe_2$ can be formed. However, for precursor (**2**), the Ni–P bond in a recyclised, and thermodynamically favoured, thio-intermediate analogous to INTF would be stronger than the Ni–S bonds, which would explain the formation of nickel phosphide. This is consistent with the corresponding Py-GC-MS at the various retention times, with peaks at Ni_2P^+: 149, NiP_2^+: 120 and NiP^+: 89.

At higher temperatures, the mechanism is less clear and we might expect that the Ni–Se bonds can also be readily dissociated. As a result, nickel would now be able to combine and deposit with a range of phosphide based species such as those arising from PNP^+: 76 and its dissociation products. The predominantly phosphide based thin films could then be observed in the high temperature LPCVD process assuming that Ni_2P is thermodynamically favoured, although we have no data to support this hypothesis.

This mechanism correlates with the observation of significant peaks at m/z 149 and 138 corresponding to Ni_2P^+ and $NiSe^+$ in the Py-GC-MS experiment for precursor (**1**). The observation of predominantly nickel phosphide or selenide films, rather than nickel sulfide films, in the CVD process at high temperature is also consistent with a greater degree of dissociation and the resultant formation of a thermodynamically favoured product. The computed homolytic dissociation energies of $NiSe_2$ or NiSe (81 and 95 kcal mol^{-1} respectively) are slightly less than those of NiS_2 or NiS (95 and 105 kcal mol^{-1} respectively) and indicate that preferential dissociation of Ni–S over Ni–Se would not be expected.

These studies provide evidence for the dissociation mechanism for all three precursors which are consistent with their LPCVD results.

Conclusions

We have used three related precursors, ligands containing S, Se, P (**1**), S, S, P (**2**) or Se, Se, P (**3**). For compound (**1**), AACVD resulted in the formation of both nickel selenide and nickel phosphide films, depending on the growth temperature and argon flow rate. LPCVD studies of this precursor (T_{prec} = 275 °C) yielded Ni_2P films at higher substrate temperatures (475–400 °C) and $Ni_{0.85}Se$ film at lower substrate temperature (375 °C). Compound (**2**) yielded only nickel sulfide films by AACVD at lower argon flow rate (140 sccm). At higher argon flow rate (200 sccm), both the phosphide and sulfide were deposited (at 525 °C), whereas at low growth temperatures (at 425 and 475 °C), only nickel sulfide films was formed. LPCVD from compound (**2**) (T_{prec} = 300 °C) gave Ni_2P films at 475–425 °C with traces of nickel sulfide at 425 °C. At lower precursor temperature (275 °C), Ni_2P films with traces of nickel sulfide was deposited at 475 °C. At 450–400 °C, increased formation of nickel sulfide along with Ni_2P was observed. Pure nickel sulfide film was not deposited under any conditions. In the case of compound (**3**) only nickel selenide films by AA-[35] and LPCVD methods were formed at all deposition temperatures. Py-GC-MS analysis coupled with density functional theory computational analysis of all three precursors provides the probable mechanism for the formation of nickel phosphide and nickel selenide films by LPCVD.

During the CVD studies, many factors control the deposition of solid phases from these precursors. What is apparent is that if the precursor has substantial residence time in the CVD reactor to generate phosphiding compounds, the phosphide can be deposited. In the mixed chalcogenide system the fact that the sulfur tends to associate, binds strongly to carbon fragments and that the selenide is present in smaller amounts than in the diseleno ligand favours the formation of phosphide at higher temperatures or greater extents of conversion of the precursor. This unusual formation of nickel selenide/sulfide or phosphide films from a single precursor is a unique feature of this system. Initial CVD studies on related cobalt compounds indicated a similar growth pattern which will be reported elsewhere.

Experimental and computational methods

The precursors $[Ni\{^iPr_2P(S)NP(Se)^iPr_2\}_2]$[8] (**1**), $[Ni\{(SP^iPr_2)_2N\}_2]$[40] (**2**) and $[Ni\{(SeP^iPr_2)_2N\}_2]$[35] (**3**) were synthesised by literature methods. Precursors (**1**) and (**2**) have a tetrahedral geometry whereas (**3**) exists in both tetrahedral and square planar forms, the tetrahedral obtained by crystallisation at room temperature has been exclusively used in our CVD studies. TGA was recorded on a Seiko SSC/S200 model instrument from 25 °C to 500 °C. Mass spectra of the precursors was recorded on a Micromass Platform II instrument by the atmospheric pressure chemical ionisation (APCI) method.

Deposition of films by LPCVD

The growth experiments were carried out in a cold wall low-pressure tube-reactor as described previously.[4e] A graphite susceptor holds a glass substrate of dimensions (1 × 1.5 cm), which was heated by a tungsten halogen lamp. A Carbolite tube furnace was used to heat the precursor (~0.20 g) under a dynamic vacuum

Published on 01 June 2010 on http://pubs.rsc.org | doi:10.1039/C002928A
Downloaded by Massachusetts Institute of Technology on 22 October 2011

(~ 10^{-2} Torr) using Edward's E2M8 vacuum pump system. Each run was carried out for 60 min and then the reactor was cooled to room temperature under vacuum.

Deposition of films by AACVD

In a typical deposition, *ca.* 0.20 g of the precursor was dissolved in 30 ml toluene for (**1**) and 30 ml THF for (**2**) and (**3**) in a two-necked 100 ml round-bottom flask with a gas inlet that allowed the carrier gas (argon) to pass into the solution to aid the transport of the aerosol. This flask was connected to the reactor tube by a piece of reinforced tubing. The argon flow rate was controlled by a Platon flow gauge. Seven glass substrates (approx. 1 × 3 cm) were placed inside the reactor tube, which is then placed in the Carbolite furnace. The substrates were heated at the desired deposition temperature for 15 min before carrying out CVD. The precursor solution in a round-bottom flask was kept in a water bath above the piezoelectric modulator of a PIFCO ultrasonic humidifier (Model No. 1077). The aerosolized droplets containing the precursor transfer with the carrier gas to the hot deposition zone. Both the solvent and the precursor flash evaporate and the precursor vapour reaches the heated substrate surface where film deposition took place. Each run was carried out for 120 min for (**1**) and 90 min for (**2**) or (**3**) and then the reactor was cooled to room temperature under an atmosphere of argon.[4k]

Characterisation of thin films

X-ray diffraction studies were performed on a Bruker AXS D8 diffractometer using a monochromated Cu-Kα radiation. The samples were mounted flat and scanned between 20 to 70° with a step size of 0.05 at a count rate of 9 s. Films were carbon coated using Edward's E306A coating system before carrying out SEM and EDX analyses. The SEM analysis was performed using a Philips XL 30FEG and EDX was carried out using a DX4 instrument. X-ray photoelectron spectroscopy (XPS) analyses were performed on a Kratos Axis Ultra XP spectrometer.

Pyrolysis GC-MS

Small quantities of precursors were dissolved in dichloromethane, 5 µl was inserted in pyrolysis tubes dried at 80 °C and analysed by normal flash pyrolysis gas chromatography mass spectrometry (Py-GC-MS). Samples were pyrolysed using a CDS (Chemical Data Systems) 5200 series pyroprobe pyrolysis unit by heating at 300 °C for 10 s. The fragments obtained were analysed using a Agilent 7890A linked to an Agilent 5975 MSD single quadrupole MS operated in electron ionisation (EI) mode (scanning between 50 and 800 atomic mass unit at 2.7 scans s^{-1}; ionisation energy 40 eV). The chromatography conditions were as follows: HP5 fused column (J+W Scientific); bonded phase 5% diphenyldimethylpoly-olsiloxane, length 30 m, inner diameter 0.32 mm; film thickness 0.25 µm. The temperature programme employed for analysis was; initial temperature 40 °C, for 2 min, followed by heating at 8 °C min^{-1} to 300 °C. The pyrolysis transfer line and injector temperatures were set at 350 °C, the heated interface at 280 °C, the EI source at 230 °C and the MS quadrupole at 150 °C. The carrier gas (helium) pressure was kept at 14 psi with flow rate of 1 cm^3 min^{-1} and the samples were introduced in split mode (split ratio 50 : 1).

Computational details

Minimum energy structures were found for reactant, intermediate and product species as shown in Fig. 19 using density functional theory (DFT), the B3LYP exchange correlation functional and the 6-31+G(d,p) basis set as implemented within the Gaussian03 program.[47,48] Single point energies were evaluated using the larger TZVP basis set for nickel and the 6-31+G(d,p) basis set for all other atoms at the stationary points obtained with the smaller basis set. Standard thermodynamic corrections were applied using the relevant partition functions, to include zero-point-energy, thermal and entropic corrections evaluated with the smaller basis set, and combined with the larger basis set potential energy differences to obtain the final reaction free energies presented in the text. Preliminary investigation demonstrated that tetrahedral structures were favoured for the high spin states for all three precursors, typical of high spin state nickel complexes. Since in each case the low spin species resulted in a square planar geometry, high spin states and tetrahedral structures were assumed for all of subsequent nickel complexes. For computational simplicity, the isopropyl groups were modelled as methyl groups throughout, and for dissociation products, neutral species and homolytic cleavage to form high spin species was also assumed, unless otherwise stated; for example, PNP was considered as a triplet diradical to represent the likely fragmentation product following breakage of the two X1-PNP-X2 bonds (Fig. S7†).

Acknowledgements

POB and MA acknowledge EPSRC, UK for financial assistance. AP, GP and KR would like to thank The University of Manchester for financial support. POB wrote this paper whilst a visiting fellow at Magdalen College, Oxford. He would like to thank the College for the Fellowship and the President and Fellows for being gracious hosts.

References

1 H. M. Manasevit, *J. Cryst. Growth*, 1981, **55**, 1.
2 A. C. Jones and P. O'Brien, *CVD of Compound Semiconductors: Precursor Synthesis, Development and Applications*, VCH, Weinheim, 1997.
3 (*a*) R. S. Mane and C. D. Lokhande, *Mater. Chem. Phys.*, 2000, **65**, 1; (*b*) A. L. Greer and N. Mathur, *Nature*, 2005, **437**, 1246.
4 (*a*) D. M. Frigo, O. F. Z. Khan and P. O'Brien, *J. Cryst. Growth*, 1989, **96**, 989; (*b*) M. A. Malik and P. O'Brien, *Chem. Mater.*, 1991, **3**, 999; (*c*) M. A. Malik, M. Motevalli, J. R. Walsh and P. O'Brien, *Organometallics*, 1992, **11**, 3136; (*d*) M. B. Hursthouse, M. A. Malik, M. Motevalli and P. O'Brien, *Polyhedron*, 1992, **11**, 45; (*e*) M. A. Malik and P. O'Brien, *Adv. Mater. Opt. Electron.*, 1994, **3**, 171; (*f*) P. O'Brien, J. R. Walsh, I. M. Watson, L. Hart and S. R. P. Silva, *J. Cryst. Growth*, 1996, **167**, 133; (*g*) P. O'Brien, J. R. Walsh, I. M. Watson, M. Motevalli and L. Henriksen, *J. Chem. Soc., Dalton Trans.*, 1996, 2491; (*h*) P. O'Brien, M. A. Malik, M. Chunggaze, T. Trindade, J. R. Walsh and A. C. Jones, *J. Cryst. Growth*, 1997, **170**, 23; (*i*) M. Chunggaze, J. McAleese, P. O'Brien and D. J. Otway, *Chem. Commun.*, 1998, 833; (*j*) M. Chunggaze, M. A. Malik and P. O'Brien, *J. Mater. Chem.*, 1999, **9**, 2433; (*k*) M. Lazell, P. O'Brien, D. J. Otway and J.-H. Park, *J. Chem. Soc., Dalton Trans.*, 2000, 4479; (*l*) N. L. Pickett and P. O'Brien, *Chem. Rec.*, 2001, **1**, 467; (*m*) M. Afzaal, D. J. Crouch, P. O'Brien, J. Raftery, P. J. Skabara, A. J. P. White and D. J. Williams, *J. Mater. Chem.*, 2004, **14**, 233; (*n*) A. Panneerselvam, M. A. Malik, P. O'Brien and J. Raftery, *J. Mater. Chem.*, 2008, **18**, 3264; (*o*) A. Panneerselvam, C. Q. Nguyen, M. A. Malik, P. O'Brien and J. Raftery, *J. Mater. Chem.*, 2009, **19**, 419.

This journal is © The Royal Society of Chemistry 2010

Published on 01 June 2010 on http://pubs.rsc.org | doi:10.1039/C002928A
Downloaded by Massachusetts Institute of Technology on 22 October 2011

5 M. Afzaal, S. M. Aucott, D. Crouch, P. O'Brien, J. D. Woollins and J.-H. Park, *Chem. Vap. Deposition*, 2002, **8**, 187.
6 (*a*) M. Afzaal, D. Crouch, M. A. Malik, M. Motevalli, P. O'Brien, J.-H. Park and J. D. Woollins, *Eur. J. Inorg. Chem.*, 2004, 171; (*b*) M. Afzaal, K. Ellwood, N. L. Pickett, P. O'Brien, J. Raftery and J. Waters, *J. Mater. Chem.*, 2004, **14**, 1310; (*c*) Y. Zhang, Y. Tang, K. Lee and M. Ouyang, *Nano Lett.*, 2009, **9**, 437.
7 (*a*) S. S. Garje, J. S. Ritch, D. J. Eisler, M. Afzaal, P. O'Brien and T. Chivers, *J. Mater. Chem.*, 2006, **16**, 966; (*b*) M. C. Copsey, A. Panneerselvam, M. Afzaal, P. O'Brien and T. Chivers, *Dalton Trans.*, 2007, 1528; (*c*) J. S. Ritch, T. Chivers, M. Afzaal and P. O'Brien, *Chem. Soc. Rev.*, 2007, **36**, 1622.
8 A. Panneerselvam, M. A. Malik, M. Afzaal, P. O'Brien and M. Helliwell, *J. Am. Chem. Soc.*, 2008, **130**, 2420.
9 S. D. Robertson, T. Chivers, J. Akhtar, M. Afzaal and P. O'Brien, *Dalton Trans.*, 2008, 7004.
10 A. Y. Matsuura, Z.-X. Shen, D. S. Dessau, C.-H. Park, T. Thio, J. W. Bennett and O. Jepsen, *Phys. Rev. B: Condens. Matter*, 1996, **53**, R7584.
11 A. F. W. Willoughby, R. Hull and P. Capper, in *Widegap II-VI Compounds for Optoelectronic Applications, Electronic Materials Series*, ed. H. E. Rúda, Chapman and Hall, London, 1992, vol. 1.
12 (*a*) K. Anuar, Z. Zulkarnain, N. Saravanan, A. Zuriyatina and R. Sharin, *Materials Science (Medžiagotyra)*, 2004, **10**, 157; (*b*) K. Anuar, Z. Zainal, N. Saravanan and S. N. Hamizi, *J. Indian Chem. Soc.*, 2005, **82**, 526.
13 M. Sharon, G. Tamizhmani, C. Levy-Clement and J. Rioux, *Sol. Cells*, 1989, **26**, 303.
14 (*a*) D. Alder, *Rev. Mod. Phys.*, 1968, **40**, 714; (*b*) J. T. Sparks and T. Komoto, *Rev. Mod. Phys.*, 1968, **40**, 752; (*c*) Ch. B. Lioutas, C. Manolikas, G. Van Tendeloo and J. Van Landyut, *J. Cryst. Growth*, 1993, **126**, 457.
15 J. Wang, S. Y. Chew, D. Wexler, G. X. Wang, S. H. Ng, S. Zhong and H. K. Liu, *Electrochem. Commun.*, 2007, **9**, 1877.
16 M. Neurock and R. A. Van Santen, *J. Am. Chem. Soc.*, 1994, **116**, 4427.
17 H. Seim, H. Fjellvåg, F. Grønvold and S. Stølen, *J. Solid State Chem.*, 1996, **121**, 400.
18 J. C. Barry and S. Ford, *J. Mater. Sci.*, 2001, **36**, 3721.
19 P. Pramanik and S. Biswas, *J. Solid State Chem.*, 1986, **65**, 145.
20 P. Pramanik and S. Bhattacharya, *J. Mater. Sci. Lett.*, 1987, **6**, 1105.
21 S. D. Sartale and C. D. Lokhande, *Mater. Chem. Phys.*, 2001, **72**, 101.
22 H. Lee, M. Kanai, T. Kawai and S. Kawai, *Jpn. J. Appl. Phys.*, 1993, **32**, 2100.
23 L. Zhang, J. C. Yu, M. Mo, L. Wu, Q. Li and K. W. Kwong, *J. Am. Chem. Soc.*, 2004, **126**, 8116.
24 S.-H. Yu and M. Yoshimura, *Adv. Funct. Mater.*, 2002, **12**, 277.
25 J. Cheon, D. S. Talaga and J. I. Zink, *Chem. Mater.*, 1997, **9**, 1208.
26 R. Nomura and H. Hayata, *Trans. Mater. Res. Soc. Jpn.*, 2001, **26**, 1283.
27 P. O'Brien, J.-H. Park and J. Waters, *Thin Solid Films*, 2003, **431–432**, 502.
28 P. O'Brien and J. Waters, *Chem. Vap. Deposition*, 2006, **12**, 620.
29 P. L. Musetha, N. Revaprasadu, M. A. Malik and P. O'Brien, *Mater. Res. Soc. Symp. Proc.*, 2005, **879E**, 1.
30 N. Alam, M. S. Hill, G. Kociok-Köhn, M. Zeller, M. Mazhar and K. C. Molloy, *Chem. Mater.*, 2008, **20**, 6157.
31 (*a*) K. Anuar, Z. Zainal, N. Saravanan and A. R. Kartini, *AJSTD*, 2004, **21**, 19; (*b*) Z. Zainal, N. Saravanan and H. L. Mien, *J. Mater. Sci.: Mater. Electron.*, 2005, **16**, 111.
32 P. Nielsen and J. J. Ritsko, *J. Appl. Phys.*, 1978, **49**, 632.
33 S. Y. Lee and P. Nash, in *Binary Alloy Phase Diagrams*, ed. T. B. Massalski, H. Okamoto, P. R. Subramanian and L. Kacprzak, ASM International, Materials Park, Ohio, 2nd edn, 1990, vol. 3, pp. 2857–2859.
34 X. Song and M. Bochmann, *J. Chem. Soc., Dalton Trans.*, 1997, 2689.
35 A. Panneerselvam, C. Q. Nguyen, J. Waters, M. A. Malik, P. O'Brien, J. Raftery and M. Helliwell, *Dalton Trans.*, 2008, 4499.
36 (*a*) F. Schrey, T. Boone, S. Nakahara, M. Robbins and A. Appelbaum, *Thin Solid Films*, 1987, **149**, 303; (*b*) J. S. Yoon, H. J. Doerr, C. V. Deshpandey and R. F. Bunshah, *J. Electrochem. Soc.*, 1989, **136**, 3513.
37 (*a*) E. Vafaei-Makhsoos, *J. Appl. Phys.*, 1980, **51**, 6366; (*b*) P. K. Ng, D. D. Snyder, J. LaSala, B. Clemens and C. Fuerst, *J. Electrochem. Soc.*, 1988, **135**, 1376.
38 (*a*) C. N. Panagopoulos, V. D. Papachristos and C. Sigalas, *J. Mater. Sci.*, 1999, **34**, 2587; (*b*) H. Li, W. Wang, H. Chen and J.-F. Deng, *J. Non-Cryst. Solids*, 2001, **281**, 31.
39 K. J. Lee and P. Nash, in *Phase Diagrams of Binary Nickel Alloys*, ed. P. Nash, ASM International, Materials Park, Ohio, 1991, pp. 235.
40 D. Cupertino, R. Keyte, A. M. Z. Slawin, D. J. Williams and J. D. Woollins, *Inorg. Chem.*, 1996, **35**, 2695.
41 Y. Okamoto, Y. Nitta, T. Imanaka and S. Teranishi, *J. Chem. Soc., Faraday Trans. 1*, 1979, **75**, 2027.
42 http://srdata.nist.gov/xps/ accessed December 2007.
43 A. B. Mandale, S. Badrinarayanan, S. K. Date and A. P. B. Sinha, *J. Electron Spectrosc. Relat. Phenom.*, 1984, **33**, 61.
44 H. W. Nesbitt, D. Legrand and G. M. Bancroft, *Phys. Chem. Miner.*, 2000, **27**, 357.
45 V. Janickis, I. Ancutienė and R. Stokienė, *Chemija*, 2009, **20**, 38.
46 P. E. M. Siegbahn, *JBIC, J. Biol. Inorg. Chem.*, 2006, **11**, 695.
47 M. J. Frisch, G. W. Trucks, H. B. Schlegel, G. E. Scuseria, M. A. Robb, J. R. Cheeseman, J. A. Montgomery, Jr., T. Vreven, K. N. Kudin, J. C. Burant, J. M. Millam, S. S. Iyengar, J. Tomasi, V. Barone, B. Mennucci, M. Cossi, G. Scalmani, N. Rega, G. A. Petersson, H. Nakatsuji, M. Hada, M. Ehara, K. Toyota, R. Fukuda, J. Hasegawa, M. Ishida, T. Nakajima, Y. Honda, O. Kitao, H. Nakai, M. Klene, X. Li, J. E. Knox, H. P. Hratchian, J. B. Cross, V. Bakken, C. Adamo, J. Jaramillo, R. Gomperts, R. E. Stratmann, O. Yazyev, A. J. Austin, R. Cammi, C. Pomelli, J. W. Ochterski, P. Y. Ayala, K. Morokuma, G. A. Voth, P. Salvador, J. J. Dannenberg, V. G. Zakrzewski, S. Dapprich, A. D. Daniels, M. C. Strain, O. Farkas, D. K. Malick, A. D. Rabuck, K. Raghavachari, J. B. Foresman, J. V. Ortiz, Q. Cui, A. G. Baboul, S. Clifford, J. Cioslowski, B. B. Stefanov, G. Liu, A. Liashenko, P. Piskorz, I. Komaromi, R. L. Martin, D. J. Fox, T. Keith, M. A. Al-Laham, C. Y. Peng, A. Nanayakkara, M. Challacombe, P. M. W. Gill, B. Johnson, W. Chen, M. W. Wong, C. Gonzalez and J. A. Pople, *Gaussian 03, Revision C.02*, 2003.
48 (*a*) C. Lee, W. Yang and R. G. Parr, *Phys. Rev. B: Condens. Matter*, 1988, **37**, 785; (*b*) R. G. Parr and W. Yang, *Density-Functional Theory of Atoms and Molecules*, Oxford University Press, Oxford, 1989; (*c*) A. D. Becke, *J. Chem. Phys.*, 1993, **98**, 5648.

This journal is © The Royal Society of Chemistry 2010